Nonlinearity-Induced Synchronization Enhancement in Micromechanical Oscillators

Dario Antonio, David A. Czaplewski, Jeffrey R. Guest, and Daniel López

Center for Nanoscale Materials, Argonne National Laboratory, Argonne, Illinois 60439, USA

Sebastián I. Arroyo and Damián H. Zanette[*]

Centro Atómico Bariloche and Instituto Balseiro, 8400 Bariloche, Río Negro, Argentina

An autonomous oscillator synchronizes to an external harmonic force only when the forcing frequency lies within a certain interval—known as the synchronization range—around the oscillator's natural frequency. Under ordinary conditions, the width of the synchronization range decreases when the oscillation amplitude grows, which constrains synchronized motion of micro- and nanomechanical resonators to narrow frequency and amplitude bounds. Here, we show that nonlinearity in the oscillator can be exploited to manifest a regime where the synchronization range *increases* with increasing oscillation amplitude. Experimental data are provided for self-sustained micromechanical oscillators operating in this regime, and analytical results show that nonlinearities are the key determinants of this effect. Our results provide a new strategy to enhance the synchronization of micromechanical oscillators by capitalizing on their intrinsic nonlinear dynamics.

Electronic components designed for time keeping and event synchronization use frequency references that, traditionally, are provided by vibrating quartz crystals. Device miniaturization, however, makes it necessary to envision the replacement of quartz crystals with simpler, fast-responding, low power-consuming elements that would be readily integrable to electronic circuits during fabrication. Because of their inherent compatibility with semiconductor technology, micromechanical oscillators are an attractive option fulfilling such requirements [1–3]. Operating at the microscale, the dynamics of these vibrating structures is often nonlinear [4,5], with large oscillation amplitudes exciting higher-order harmonics in the oscillatory motion. It is therefore of critical importance for functional design to characterize the effect of such nonlinearities, in particular, on the oscillator's capability to synchronize with external signals. In this Letter, we show that, under suitable conditions, nonlinearities can, in fact, improve the synchronization properties of micromechanical oscillators.

Synchronized motion of an autonomous oscillator, with the same frequency as an externally applied harmonic perturbation, is arguably the most basic form of coherent response of a physical system to an external action. Generally, synchronization is possible when the frequency of the external perturbation Ω_s lies close enough to the oscillator's frequency Ω_0, such that $|\Omega_s - \Omega_0| < \Delta\Omega$ where $2\Delta\Omega$ is the synchronization range. Intuitively, it is observed that the synchronization range increases as the intensity of the harmonic perturbation is increased [6]; i.e., the larger the interaction with the external perturbation, the further the frequency can be shifted. It is also usually observed that the width of the synchronization range decreases with

increasing oscillator amplitude; i.e., as the self-sustained drive force of the primary oscillator is increased, the ability to change the frequency of operation through synchronization to an external harmonic perturbation decreases. Here, we show that, contrary to an oscillator operating in the linear regime, for a self-sustained mechanical oscillator driven into the nonlinear regime, synchronization by an external force is *enhanced* as the amplitude of its self-sustained oscillations increases. We demonstrate this counterintuitive effect experimentally, through the use of an electrically driven micromechanical oscillator in a closed-loop configuration and an external oscillator with a tunable frequency. A theoretical model reveals that the enhancement of synchronizability is a direct consequence of nonlinearities.

A schematic of the circuit used to drive the micromechanical oscillator is shown in Fig. 1(a), where a closed feedback circuit compensates for intrinsic damping to maintain self-sustained oscillations [7]. The micromechanical oscillator used for these measurements is a silicon structure composed of three interconnected parallel beams, 500 μm long, clamped at their two ends [8]; as we will show below, this resonator can be driven deep into the nonlinear regime. In its principal oscillation mode, transverse displacement is detected capacitively by means of a comb-drive electrode. After amplification, the resulting signal is conditioned by shifting its phase by a prescribed amount ϕ_0 and fixing its amplitude V_0. The conditioned signal is then reinjected through another comb-drive electrode as a driving capacitive force that is time varying and proportional to $V_{dc}V(t)$ [where $V_{dc} \approx 5$ V $\gg V(t)$]; therefore, applied forces $F(t)$ are proportional to the

applied drive voltages $V(t)$. In the absence of any other force, this closed loop sustains the beam's vibration at an amplitude A_0 and a frequency Ω_0 determined by its mechanical properties, the phase shift ϕ_0, and the voltage V_0. The amplitude grows with V_0 and, as in other resonating mechanical systems, attains a maximum when the driving force is in phase with the oscillation velocity. This resonance condition is achieved in the phase shifter by advancing the oscillating signal by $\phi_0 = \pi/2$. Because of the hardening nonlinearity in the dynamics of the oscillator (see below), the frequency of self-sustained oscillations Ω_0 increases as V_0 increases. External perturbation—aimed to entrain the oscillator into synchronized motion—consists of a voltage signal of amplitude V_s and frequency Ω_s, which is added to the self-sustaining signal. The oscillation frequency of the micromechanical oscillator is measured on the conditioned signal at the exit of its amplitude control [see Fig. 1(a)].

The motion of the principal oscillation mode is well described by Newton's equation for a normal coordinate $x(t)$ (representing displacement from equilibrium) with a cubic nonlinear term, namely, Duffing's equation [10]

$$m\ddot{x} + \gamma\dot{x} + kx + k_3 x^3 = F_0 \cos(\phi + \phi_0) + F_s \cos\Omega_s t, \tag{1}$$

where m, γ, k, k_3, F_0, and F_s are the effective mass, damping coefficient, elastic constant, cubic-force coefficient, self-sustaining force, and external perturbation, respectively. The external perturbation used for synchronization enters the equation of motion as an external forcing term. Normalizing by the spring constant k and choosing time units such that the natural frequency of the principal mode equals unity ($t\sqrt{k/m} \to t$), the equation of motion reads

$$\ddot{x} + Q^{-1}\dot{x} + x + \beta x^3 = f_0 \cos(\phi + \phi_0) + f_s \cos\Omega_s' t, \tag{2}$$

where $Q = \sqrt{km}/\gamma$ is the quality factor, $\beta = k_3/k$, $f_0 = F_0/k$, $f_s = F_s/k$, and $\Omega_s' = \Omega_s/\sqrt{k/m}$. The cubic-term coefficient β is positive (negative) for hardening (softening) nonlinearities. The amplitude f_0 and (advanced) phase shift ϕ_0 of the self-sustaining force determine the conditioning of the feedback signal. We focus on the case $\phi_0 = \pi/2$, where the effect of the self-sustaining force is maximal. The angle $\phi(t)$ is the instantaneous oscillation phase of the coordinate $x(t)$. The synchronization force f_s is applied with a tunable frequency Ω_s'. Analytical and numerical methods to treat Eq. (2) when $\beta = 0$ have been discussed elsewhere [11]. When $\beta \neq 0$, the cubic term is handled using the standard treatment of weak nonlinearities [6], by neglecting higher-harmonic contributions. In the measurement, the force amplitudes f_0 and f_s are proportional to the voltages V_0 and V_s, respectively.

With no applied synchronization force ($f_s = 0$), we take $x(t) = A_0 \cos\phi = A_0 \cos\Omega_0' t$ and find that the system
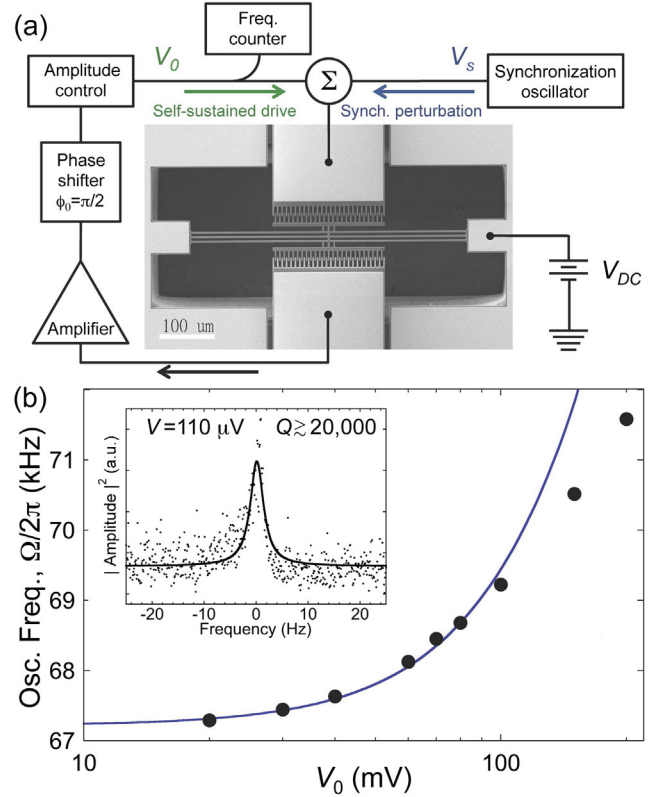

FIG. 1 (color online). Nonlinear MEMS device. (a) Schematic of the experimental setup. The closed-loop circuit, which amplifies and conditions the displacement signal read from the oscillator, maintains the system in self-sustained oscillation. An external synchronization signal is also fed to the oscillator. The scanning electron microscope image shows the clamped-clamped oscillator. (b) Measured frequency of the oscillator versus applied self-sustained drive voltage V_0 and no synchronization drive ($V_s = 0$); blue curve shows the fit to Eq. (3) for $V_0 \leq 100$ mV. Inset shows a least-squares Lorentzian fit to the amplitude squared of a frequency sweep under weak excitation ($V = 110$ μV), revealing $Q \gtrsim 20\,000$ [9].

attains oscillations whose frequency Ω_0' and amplitude A_0 (see the Supplemental Material [12]) can be given explicit expressions

$$\Omega_0' = \frac{1}{\sqrt{2}}[1 + (1 + 3\beta Q^2 f_0^2)^{1/2}]^{1/2},$$

$$A_0 = Qf_0/\Omega_0'. \tag{3}$$

As seen in Fig. 1(b), our resonator, which is characterized by $Q \gtrsim 20\,000$ [9] at low amplitude (inset), is well described by Eq. (3) for driving voltages $V_0 \lesssim 100$ mV. Noting that $f_0 \propto V_0$, we fold the oscillator's mechanical parameters into a parameter α by defining $\alpha V_0 = |\beta|^{1/2}Qf_0$; the fit for $V_0 \leq 100$ mV in Fig. 1(b) reveals $\alpha = 3.1 \pm 0.1$ V^{-1} and the natural frequency $\sqrt{k/m} = 2\pi \times 67.22$ kHz. Note that the self-sustained frequency is only significantly different from the natural frequency for

$|\beta| f_0^2 \gtrsim Q^{-2}$; this occurs deep in the nonlinear regime when the magnitude of the nonlinear term ($\sim |\beta| A_0^3$) becomes comparable to or larger than the linear term ($\sim A_0$).

Under the action of the external synchronization perturbation $f_s \neq 0$, we find that synchronized solutions exist when Ω_s' lies within an interval $\Omega_0' \pm \Delta\Omega'$. We can define this interval as a function of the ratio between the synchronization and self-sustaining force $p = f_s/f_0$ such that $\Delta\Omega' = p\delta\Omega_c'$. Taking $p = f_s/f_0 \ll 1$, $Q \gg 1$, and inserting into Eq. (2), this interval can be shown (see the Supplemental Material [12]) to take the form

$$\Delta\Omega' = p\delta\Omega_c' = \frac{p}{2Q}\left[\left(\frac{3Q\beta A_0^2}{2\Omega_0'}\right)^2 + 1\right]^{1/2}. \quad (4)$$

Note that $\Delta\Omega'$ is not directly dependent on the sign of the nonlinear coefficient β (it is weakly dependent through Ω_0').

Through Eq. (4), we can see that, in the case of a linear oscillator ($\beta = 0$), the synchronization range $2\Delta\Omega' = p/Q$ is simply proportional to the linewidth of the resonant response (Q^{-1}) and the ratio of the synchronization force to the self-sustained force (p). This dependence is consistent with a competition between forces: a stronger synchronization force increases the synchronization range, while a stronger self-sustaining force decreases the synchronization range. However, in the case of a nonlinear oscillator ($\beta \neq 0$), we see that this range can grow once the first term in the brackets in Eq. (4) becomes comparable to 1; using Eq. (3) and noting that $\Omega_0' \approx 1$, we see that this occurs for $|\beta| f_0^2 \gtrsim Q^{-3}$. This corresponds to the regime where the nonlinear term ($\sim |\beta| A_0^3$) becomes comparable to or larger than the dissipative force ($\sim A_0/Q$); for large Q, this is achieved for considerably lower amplitudes (and forces) than needed to reach the strongly nonlinear regime described above.

We explore the amplitude dependence of the synchronization range of our nonlinear oscillator in Fig. 2, where in Fig. 2(a) we plot the measured oscillation frequency versus the applied synchronization frequency Ω_s for various applied self-sustained and synchronization forces, where we hold the ratio of the two forces constant for simplicity ($p = f_s/f_0 = V_s/V_0 = 0.05$ and $\phi_0 \lesssim \pi/2$). For each pair (V_0, V_s), we sweep Ω_s both upwards (blue) and downwards (red); note that the natural frequency Ω_0 of the oscillator shifts as shown in Fig. 1(b) as a function of V_0. Along the upward sweep, the oscillator synchronizes with the external forcing when Ω_s reaches the vicinity of Ω_0. Above that point, the oscillation frequency is identical to Ω_s up to about 1 part in 10^5 (data on the graph's diagonal). Further increase of Ω_s, however, leads to sudden desynchronization at $\Omega_0 + \Delta\Omega$. Along the downward sweep, synchronization persists until Ω_s reaches $\Omega_0 - \Delta\Omega$. In both directions, the sharp desynchronization transition occurs within an interval of < 1 Hz, the size of incremental frequency change. When synchronized, fluctuations in the oscillation frequency are
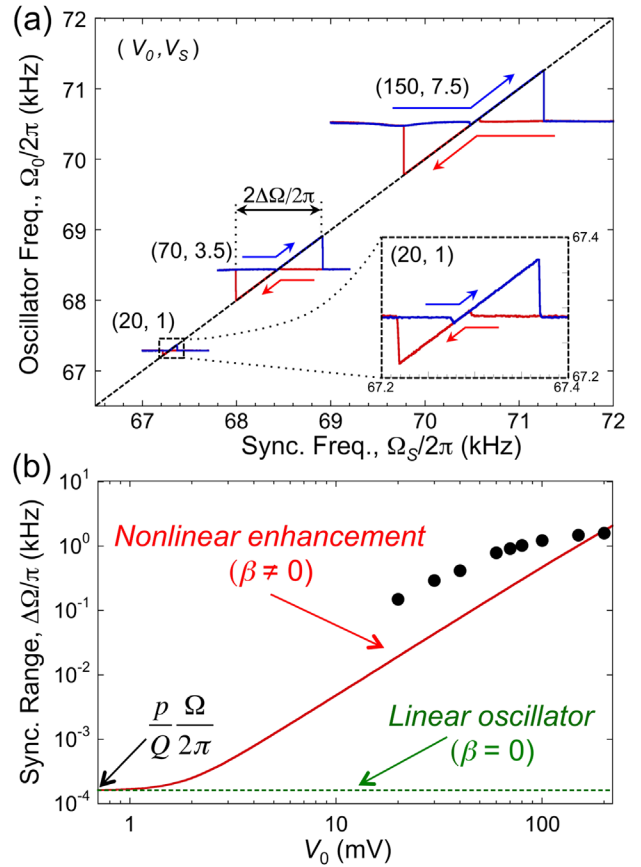

FIG. 2 (color online). Synchronization behavior. (a) Measured oscillation frequency versus synchronization frequency ($\Omega_s/2\pi$) for the oscillator, measured for $p = 0.05$ and three values of the applied voltages. The corresponding pairs (V_0, V_s), measured in mV, are indicated by labels. Data over the graph's diagonal correspond to synchronized oscillations. The arrows stand for the direction in which the synchronization frequency was changed during each run of the experiment. The (20,1) trace is shown in detail in the inset. (b) Measured synchronization range as a function of V_0 ($p = 0.05$) for experimental data sets as shown in (a); uncertainty and repeatability in the measured synchronization ranges are smaller than the size of the data points. Red curve shows the predicted behavior from Eq. (4), where we have taken $Q = 20\,000$. The green dotted line shows the prediction for a linear oscillator ($\beta = 0$).

reduced because of the low noise level in the external oscillator, in this case, a signal generator [13]. It is evident in these traces that the synchronization range is increasing with increasing force despite the fact that the ratio between the forces p is fixed.

In Fig. 2(b), we plot the width of the observed synchronization range ($2\Delta\Omega$) for our device as a function of the self-sustained drive voltage V_0 for $p = 0.05$ ($V_s = pV_0$). Our measured synchronization range increases with drive voltage and is almost *4 orders of magnitude larger* than expected for a linear oscillator ($\beta = 0$, dotted green line). In order to understand the correlation with theory, we also plot the theoretical prediction of the synchronization range

(red line) from Eq. (4) by employing the measured parameters for our device; we have used the substitution for A_0 [Eq. (3)], the measured values for $\sqrt{k/m}$ and Q, and the fit value of $\alpha = 3.1$ V^{-1} found from Fig. 1(b) (where we have again used the substitution $\alpha V_0 = |\beta|^{1/2} Q f_0$). There are no adjustable parameters in this curve. As seen in the figure, the dependence of the measured synchronization range on the drive voltages agrees qualitatively with the predicted values; indeed, the measured synchronization range is significantly larger than the prediction, indicating that the Duffing equation does not provide a complete description of the closed loop and synchronized response of the nonlinear oscillator for large self-sustaining amplitudes. In addition, in this high amplitude and highly nonlinear regime, several factors may contribute to this discrepancy including amplitude-dependent device parameters such as α and Q, higher-order nonlinearities and harmonics in both the device dynamics and the drive and signal transduction (through the comb electrodes), and our use of a finite synchronization force f_S (through p), which may affect the synchronization range more dramatically than we account for in our perturbative treatment. This breakdown becomes clearer for $V_0 > 100$ mV, where the measured synchronization range begins to saturate and the behavior deviates qualitatively from the prediction; this is consistent with the deviation of the measured device frequency shown in Fig. 1(b) from Eq. (3) in this voltage range. Drive voltages below $V_0 \sim 20$ mV are challenging to measure for our highly nonlinear oscillator and with our experimental setup because self-sustained oscillations are not stable in this range; however, we believe the synchronization range will decrease with reduced drive voltages as suggested by the theory until it reaches the well-understood linear regime.

In order to get a clearer picture of this surprising behavior, in Fig. 3 we plot the synchronization range $2\Delta\Omega'$ as a function of both $|\beta|^{1/2} f_0$ and Q as predicted by Eqs. (3) and (4). Three regions spanning orders of magnitude in synchronization range are clearly observable and can be understood by the comparative strength of the nonlinear term to the other terms in Duffing's equation [Eqs. (1) and (2)]. On the left of the plot, when $|\beta| f_0^2 \lesssim Q^{-3}$, the nonlinear term ($\beta A_0^3$) is smaller than both the dissipative term (A_0/Q) and the elastic term (A_0) and the synchronization behavior is characterized by a linear response. When $Q^{-3} \lesssim |\beta| f_0^2 \lesssim Q^{-2}$, the nonlinear term dominates the dissipative term but is still small compared to the elastic term; this regime shows rapid increase of the synchronization range with increasing nonlinearity or self-sustained driving force as demonstrated by the measurements of our oscillator. Once $|\beta| f_0^2 \gtrsim Q^{-2}$, indicating the nonlinear force dominates even the elastic force, the oscillator is deep in the nonlinear regime and the rate of increase of the synchronization range is slowed by the increase in the self-sustained frequency due to the increase (for $\beta > 0$) in Ω' as indicated by Eq. (3).
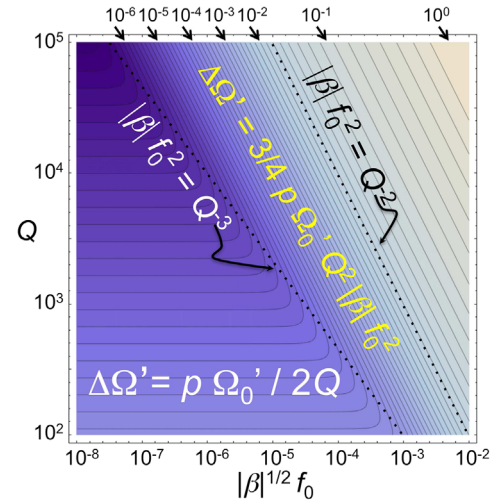

FIG. 3 (color online).   Contour plot of the synchronization range $\Delta\Omega'$ predicted by Eq. (4) as a function of $|\beta|^{1/2} f_0$ and Q for $p = 0.05$. The various regions are labeled and separated by dotted lines.

Our results show that the Duffing model gives a good description of the micromechanical oscillator for $V_0 \lesssim 100$ mV. Both the nonlinear self-sustained frequency and the increase in the synchronization range with increasing self-sustained force are well predicted by the model. We can estimate the nonlinearity in our device by quantifying the strength of the applied forces; by using $V_{dc} = 5$ V, the physical parameters of our structure, and the forces expected in a parallel-plate comb drive, we estimate that $f_0/V_0 = 2.6 \times 10^{-10}$ m/V. Using this, we can estimate its nonlinear coefficient: $\beta = 1.5 \times 10^{19}$ V^2/m$^2 \times \alpha^2/Q^2$. For our measured value of $Q \gtrsim 20\,000$ and fit for $\alpha = 3.1$ V^{-1}, we arrive at $\beta \lesssim 3.3 \times 10^{11}$ m^{-2}. Because of its ability to access large nonlinearities, the oscillator under study was well suited to probe this surprising regime of nonlinear synchronization. On the other hand, we have found that driving the oscillator with higher voltages causes the response to deviate from the behavior predicted by the Duffing equation. Large-amplitude oscillations appear to be dominated by higher-order nonlinear effects.

The regime of synchronization enhancement disclosed in this Letter, which may also be related to the sudden increase of the synchronization range mentioned in a recent publication for two coupled micro-oscillators [14,15], is a beneficial effect of nonlinearity on the coherent response of an oscillator to an external action. It may find advantageous applications in devices where many oscillators must be synchronized by a master signal, such as in array of resonators for optical processing and communications systems [16,17], by widening the domain where synchronized motion occurs. Extending the same effect to the mutual entrainment of two or more oscillators could assist in the development of a solution to some of the problems associated with the use of micromechanical oscillators in

miniaturized devices. First, the undesired dependence of the oscillation frequency with the amplitude—namely, the amplitude-frequency effect [4,5], due to the nonlinear nature of the individual dynamics—might be compensated, at least partially, by bidirectionally coupling oscillators with hardening and softening nonlinearities. Second, the effect of thermal noise [7,18] may be reduced by producing a more robust signal from the synchronization of several oscillators with similar self-sustained frequencies.

---

[*]Also at Consejo Nacional de Investigaciones Científicas y Técnicas, Argentina.

[1] K. L. Ekinci and M. L. Roukes, Rev. Sci. Instrum. **76**, 061101 (2005).

[2] C. T. C. Nguyen, IEEE Trans. Ultrason. Ferroelectr. Freq. Control **54**, 251 (2007).

[3] J. T. M. van Beek and R. Puers, J. Micromech. Microeng. **22**, 013001 (2012).

[4] M. Agarwal, H. Mehta, R. N. Candler, S. Chandorkar, B. Kim, M. A. Hopcroft, R. Melamud, G. Bahl, G. Yama, T. W. Kenny *et al.*, J. Appl. Phys. **102**, 074903 (2007).

[5] M. Agarwal, S. A. Chandorkar, H. Mehta, R. N. Candler, B. Ki, and M. A. Hopcroft, Appl. Phys. Lett. **92**, 104106 (2008).

[6] A. H. Nayfeh and D. T. Mook, *Nonlinear Oscillations* (Wiley, New York, 1995).

[7] B. Yurke, D. S. Greywall, A. N. Pargellis, and P. A. Busch, Phys. Rev. **51**, 4211 (1995).

[8] D. Antonio, D. H. Zanette, and D. López, Nat. Commun. **3**, 806 (2012).

[9] We report a lower limit for Q because the residual asymmetry in the measured line shape indicates that the Duffing nonlinearity is artificially broadening the line.

[10] J. Guckenheimer and P. Holmes, *Nonlinear Oscillations, Dynamical Systems, and Bifurcations of Vector Fields* (Springer, New York, 1983).

[11] S. I. Arroyo and D. H. Zanette, Phys. Rev. E **87**, 052910 (2013).

[12] See the Supplemental Material at http://link.aps.org/supplemental/10.1103/PhysRevLett.114.034103 for a more compete analysis of the forced self-sustained Duffing oscillator and a geometrical description of the micro mechanical oscillator.

[13] A. Pikovsky, M. Rosemblum, and J. Kurths, *Synchronization: A Universal Concept in Nonlinear Sciences* (Cambridge University Press, Cambridge, 2003).

[14] D. K. Agrawal, J. Woodhouse, and A. A. Seshia, Phys. Rev. Lett. **111**, 084101 (2013).

[15] M. H. Matheny, M. Grau, L. G. Villanueva, R. B. Karabalin, M. C. Cross, and M. L. Roukes, Phys. Rev. Lett. **112**, 014101 (2014).

[16] C. T. C. Nguyen, L. P. B. Katehi, and G. M. Rebeiz, Proc. IEEE **86**, 1756 (1998).

[17] M. Zhang, G. S. Wiederhecker, S. Manipatruni, A. Barnard, P. McEuen, and M. Lipson, Phys. Rev. Lett. **109**, 233906 (2012).

[18] P. Ward and A. Duwel, IEEE Trans. Ultrason. Ferroelectr. Freq. Control **58**, 195 (2011).